DMD Fast Forward. Published on January 29, 2015 as DOI: 10.1124/dmd.114.061879
This article has not been copyedited and formatted. The final version may differ from this version.

DMD # 61879

IDENTIFICATION OF GLUTATHIONE CONJUGATES OF ACETYLENE-CONTAINING POSITIVE ALLOSTERIC MODULATORS OF METABOTROPIC GLUTAMATE RECEPTOR SUBTYPE 5

XIAOLIANG ZHUO, XIAOHUA STELLA HUANG, ANDREW P. DEGNAN, LAWRENCE B. SNYDER, FUKANG YANG, HONG HUANG, YUE-ZHONG SHU, BENJAMIN M. JOHNSON

Department of Biotransformation (X.Z., B.M.J.), Discovery Analytical Sciences (X.S.H.), Neuroscience Chemistry (A.P.D., L.B.S., F.Y., H.H.), Bristol-Myers Squibb Co., 5 Research Parkway, Wallingford, CT 06492

Department of Biotransformation (Y.-Z.S.), Bristol-Myers Squibb Co., Route 206 & Province Line Road, Princeton, NJ 08543

Running Title: GSH conjugation of acetylene-containing mGluR5 PAMs

Correspondence should be addressed to:

Xiaoliang Zhuo, Discovery Biotransformation, Bristol-Myers Squibb Co., 5 Research Parkway, Wallingford, CT 06492

Tel: (203) 677 5938; Fax: (203) 677 6193; e-mail: xiaoliang.zhuo@bms.com

Number of Text Pages: 18

Number of Tables: 3

Number of Figures: 11

Number of References: 24

Number of words: 232 (Abstract)

713 (Introduction)

1495 (Discussion)

Abbreviations used are: P450, cytochromes P450; DMSO, dimethyl sulfoxide; GSH, glutathione; GST, glutathione *S*-transferase; HPLC, high pressure liquid chromatography; MS, mass spectrometry; NADPH, β-Nicotinamide adenine dinucleotide phosphate tetrasodium salt; UV, ultraviolet.

Abstract

A recent medicinal chemistry campaign to identify positive allosteric modulators (PAMs) of metabotropic glutamate receptor subtype 5 (mGluR5) led to the discovery of potent compounds featuring an oxazolidinone structural core flanked by biaryl acetylene and haloaryl moieties. However, biotransformation studies of some of these mGluR5 PAMs demonstrated the formation of glutathione (GSH) conjugates. The conjugates in question were formed independently of NADPH as the main products in liver microsomes and liver cytosol (rat and human) and exhibited masses that were 307 u greater than their respective substrates, indicating the involvement of a reductive step in the formation of these metabolites. To further characterize the relevant metabolic sequences, GSH conjugates of (4*R*,5*R*)-5-(3-fluorophenyl)-4-(5-(pyrazin-2-ylethynyl)pyridin-3-yl)oxazolidin-2-one and (4*R*,5*R*)-5-(4-fluorophenyl)-4-(6-((3-fluoropyridin-2-yl)ethynyl)pyridin-2-yl)oxazolidin-2-one were biosynthesized and isolated. Subsequent analysis by NMR showed that GSH had reacted with the acetylene carbon atoms of these mGluR5 PAMs, suggesting a conjugate addition mechanism and implicating cytosolic and microsomal glutathione *S*-transferases (GSTs) in catalysis. Interestingly, five closely related mGluR5 PAMs were not similarly prone to the formation of GSH conjugates in vitro. These compounds also featured acetylenes, but were flanked by either phenyl or cyclohexyl rings, indicating that the formation of GSH conjugates was influenced by proximal functional groups that modulated the electron density of the triple bond and/or differences in enzyme-substrate specificity. These results informed an ongoing drug-discovery effort to identify mGluR5 PAMs with drug-like properties and a low risk of reactivity with endogenous thiols.

Introduction

mGluR5 is one of eight known metabotropic glutamate receptors and is mainly expressed in the postsynaptic membrane of glutamatergic neurons and glial cells. Once activated, mGluR5 enhances function of the *N*-methyl-D-aspartate (NMDA) receptor, an ionotropic glutamate receptor and a signaling partner associated with mGluR5 (Awad et al., 2000; Pisani et al., 2001; Lindsley et al., 2006; Perroy et al., 2008). mGluR5 potentiators have conferred antipsychotic properties and improved cognitive function in rodent models, suggesting their potential utility in the treatment of the positive and cognitive symptoms of schizophrenia (Marino and Conn, 2002; Kinney et al., 2003; Liu et al., 2008; Conn et al., 2009). In an effort to address this area of unmet medical need, multiple positive allosteric modulators (PAMs) of mGluR5 were prepared and characterized at Bristol-Myers Squibb. These compounds, which lacked intrinsic agonistic activity but selectively potentiated glutamate-induced activation of mGluR5 via binding to allosteric transmembrane domains of the receptor, featured high binding affinity, subtype selectivity, and excellent in vitro activity in a functional assay. The structures of these potent compounds included an oxazolidinone core substituted at C-4 and C-5 with aryl groups. The aryl group at C-4 was further substituted by an aryl- or alkyl-acetylene.

As a pharmacophore, acetylene has been used in a variety of pharmaceutical agents including oral contraceptives (e.g.17α-ethynylestradiol), HIV-1 reverse transcriptase inhibitors (e.g. efavirenz), anti-fungal drugs (e.g. terbinafine), and inhibitors of the epidermal growth factor receptor tyrosine kinase (e.g. erolotinib). In addition, acetylene is also a structural component present in pyrethroid insecticides (e.g. Etoc). It

has been well documented that reactive intermediates formed via acetylene bioactivation may result in mechanism-based P450 inactivation and, in cases where the metabolite is able to diffuse from the active site of P450, may covalently modify macromolecules such as cellular proteins and potentially initiate subsequent biological events leading to toxicity (Kalgutkar et al., 2005; Ortiz de Montellano, 2005).

On the other hand, a growing body of evidence demonstrates that acetylene groups may conjugate with glutathione (GSH) through nucleophilic addition, yielding ethenethiol products. When Tomigahara and colleagues studied the metabolite profile of Etoc in rat urine, they identified an *N*-acetylcysteine conjugate that was formed by *O*-dealkylation, addition of GSH to the terminal acetylenic carbon and then processing along the mercapturic acid pathway (Tomigahara et al., 1994). Importantly, it was postulated that the GSH conjugate that was formed as an intermediate in this sequence was the product of glutathione *S*-transferase enzymes (GST). As a second example, efavirenz and its analogs (DPC961 and DPC963) were subject to hydroxylation and sulfonation followed by reaction of the internal acetylene moiety with one or two molecules of GSH. These metabolites were further processed to cysteinylglycine products that were observed in rat urine and bile (Mutlib et al., 1999a; Mutlib et al., 1999b; Chen et al., 2002). The addition of GSH to the acetylene was later recapitulated using a metabolic precursor in the presence of both hepatic and renal S9 fractions of the rat, as well as isolated GSTs, demonstrating the catalytic activity of these enzymes. In a third example, a synthetic standard of a propargyl aldehyde metabolite of terbinafine (TBF-A) was found to undergo chemical conjugation with GSH across the acetylenic carbon via 1,6-Michael addition (Iverson and Uetrecht, 2001). The authors further

suggested that the GSH conjugate might help transport the electrophilic TBF-A across the hepatocyte canalicular membrane and then release it on site, implicating biliary accumulation of TBF-A in cases of cholestatic hepatitis presented by patients treated with terbinafine.

Either scenario, metabolic activation by P450s or conjugation with GSH to deplete the cellular protective reagent, could initiate a cascade of events resulting in adverse biological effects. During lead optimization in drug discovery, biotransformation assays including metabolite profiling and GSH trapping in vitro were used to assess bioactivation associated with structural alerts, including the acetylene. The results provided information to guide structural modification by medicinal chemistry in the interest of avoiding problematic features.

In the present study, the potential of eight structurally related acetylene-containing mGluR5 PAMs to form GSH conjugates was assessed using subcellular liver fractions (rat, human). The GSH conjugates of two compounds were isolated, and their structures were elucidated by NMR. The influence of structural features on reactivity toward GSH, as well as species-related differences in extents of conjugate formation, are also reported and discussed.

Materials and Methods

Chemicals and Liver Subcellular Fractions Reduced β-nicotinamide adenine dinucleotide phosphate tetrasodium salt (NADPH), glutathione (GSH), potassium phosphate (monobasic and dibasic), and formic acid were purchased from Sigma (St Louis, MO). HPLC-grade water and acetonitrile were obtained from Mallinckrodt Baker

(Phillipsburg, NJ). Liver microsomes and liver S9 fractions (rat and human) and liver cytosol (rat) were obtained from BD Biosciences (Bedford, MA). Human liver cytosol was purchased from Xenotech (Lenexa, KS). (4*R*,5*R*)-5-(3-Fluorophenyl)-4-(5-(pyrazin-2-ylethynyl)pyridin-3-yl)oxazolidin-2-one (**1**), (4*R*,5*R*)-5-(4-fluorophenyl)-4-(6-((3-fluoropyridin-2-yl)ethynyl)pyridin-2-yl)oxazolidin-2-one (**2**), (4*R*,5*R*)-5-(3,5-difluorophenyl)-4-(5-((5-fluoropyridin-3-yl)ethynyl)pyridin-3-yl)oxazolidin-2-one (**3**), (4*R*,5*R*)-5-(2,3-difluorophenyl)-4-(5-(phenylethynyl)pyridin-3-yl)oxazolidin-2-one (**4**), (4R,5R)-5-(3-fluorophenyl)-4-(2-methoxy-5-(phenylethynyl)pyridin-3-yl)oxazolidin-2-one (**5**), (4*R*,5*R*)-4-(5-((3-chlorophenyl)ethynyl)pyridin-3-yl)-5-(2,6-difluorophenyl)oxazolidin-2-one (**6**), (4*R*,5*R*)-4-(3-(phenylethynyl)phenyl)-5-(pyridin-3-yl)oxazolidin-2-one (**7**), and (4*R*,5*R*)-4-(5-(cyclohexylethynyl)pyridin-3-yl)-5-(2,5-difluorophenyl)oxazolidin-2-one (**8**) (Figure 1) were synthesized and characterized by Bristol-Myers Squibb (Wallingford, CT).

***In Vitro* Metabolism** Reaction mixtures (0.5 mL) contained either liver microsomes (1 mg/mL) or cytosol (1 mg/mL) of rat or human, heat-inactivated liver S9 fractions (2 mg/mL) of rat or human, or no liver subcellular fractions. Other components included potassium phosphate buffer (100 mM, pH 7.4), substrate (10 μM), and either NADPH (1 mM) and GSH (5 mM) for microsomal incubations or GSH (5 mM) alone for all other incubations. The reactions were prepared using a liquid handler (Tecan Freedom EVO, Männedorf, Switzerland) and incubated at 37 °C. At 0 and 30 min, aliquots (150 μL) of reaction mixture were collected, and reactions were terminated by adding three volumes of acetonitrile. Proteins were then removed using a Phenomenex (Torrance, CA) Strata filter plate by centrifugation (Eppendorf 5804 R, Hamburg, Germany) at 2000*g* for

3 min. The filtrate was collected in a 96-well plate and evaporated to 25% of the original volume under N_2 gas. The remaining aqueous phase was analyzed using HPLC/UV/MS.

HPLC/UV/MS The HPLC/UV/MS system consisted of a Waters Acquity binary solvent manager, a Waters Acquity sample manager, a Waters Acquity photodiode array detector, and a Waters Xevo Q-TOF mass spectrometer (Waters Corporation, Milford, MA). Chromatographic separations were carried out on a Waters BEH C18 column (1.7 μm, 2.1 × 100 mm). The mobile phase consisted of water/acetonitrile/formic acid (95/5/0.1, v/v/v) (solvent A) and acetonitrile (solvent B) at a flow rate of 0.5 mL/min with a linear gradient as follows: 2% B isocratic for 1 min, 2% to 35% B over 5.5 min, and finally 35% to 100% B over 3.5 min. The gradient was maintained for 1 min and then returned to initial conditions for a 1.5-min equilibration period. Eluent from the column was analyzed by the photodiode array detector (scanning 200 – 400 nm at 5 Hz) followed by the mass spectrometer equipped with an electrospray ionization source and operated in positive-ion mode. To obtain maximum sensitivity based on the ionization of the parent molecules, the source temperature was 125 °C, the desolvation temperature was 250 °C, the capillary voltage was 3 kV, the sampling cone was 30 (arbitrary units) and the extraction cone was 1.7 (arbitrary units). All mass spectrometry data was acquired using a low collision voltage (6 V) and a high-voltage ramp (25 – 40 V), and data was processed using Metabolynx software (Waters Corp). Metabolite structures were assigned based on their LC/MS/MS product-ion mass spectra.

Relative abundances of drug-related components detected in the incubations were estimated according to their UV peak areas at the maximum absorption wavelength (λ =

303 nm) of the corresponding parent drug. Molar extinction coefficients of compounds and their metabolites were assumed to be similar.

Isolation of GSH Conjugates of 1 and 2 GSH conjugates of **1** and **2** were biosynthesized in an incubation (5 mL) containing potassium phosphate buffer (100 mM, pH 7.4), Aroclor 1254-induced rat liver S9 (4 mg/mL), substrate (600 μM) and GSH (4 mM). The reaction was incubated at 37 °C for 2 h. The reaction was stopped with the addition of 2 volumes of acetonitrile followed by centrifugation (Eppendorf 5804 R) at 1500*g* for 10 min. Supernatant was removed to a glass vial and dried using nitrogen gas. Residues were resuspended in 500 μL of solvent containing water/acetonitrile/formic acid (90/10/0.1, v/v/v) and then analyzed using an HPLC/UV system (the same system used for metabolite analysis) coupled with an Agilent 1100 fraction collector (Agilent Technologies, Santa Clara CA). The HPLC elution method for the separation of GSH conjugates was the same as mentioned in the HPLC/UV/MS section. Selected HPLC fractions containing metabolites of interest were then dried under nitrogen gas.

NMR Analysis The isolated GSH conjugates (10 to 100 μg) were dissolved in 50 μL or 160 μL of DMSO-d_6 and transferred to 1.7-mm or 3-mm NMR tubes. All ^{1}H spectra were acquired on a Bruker Avance 500 MHz spectrometer (Bruker BioSpin Corporation, Billerica, MA) equipped with a 5-mm TCI cryo probe, and ^{13}C spectra were acquired at 125 MHz on the same instrument. The chemical shifts were referenced to the residual solvent (DMSO-d_6) signals of 2.49 and 39.5 ppm for ^{1}H and ^{13}C, respectively. The two dimensional spectra, including heteronuclear multiple quantum coherence (HMQC), heteronuclear multiple bond correlation (HMBC), and rotating frame

Overhauser enhancement spectroscopy (ROESY) experiments, were acquired according to standard protocols provided by the instrument manufacturer.

Results

Formation of GSH conjugates The propensity of compounds **1 – 8** to form GSH conjugates was evaluated in enzyme-free assays (potassium phosphate buffer or heat-inactivated liver S9) and in incubations with liver microsomes or cytosol (human and rat). The amounts of GSH conjugates detected following 30-min incubations were expressed in terms of percent turnover relative to the amounts of the corresponding parent drug at 0 min based on UV peak areas (Table 1). Since multiple conjugates of **1** and **2** were observed, cumulative levels of GSH conjugates were calculated and reported for each compound.

The reactivity of compound **1** with GSH was evaluated in enzyme-free incubations or with liver subcellular fractions. Three GSH conjugates (P + 307 u), GSH1-1, GSH1-2, and GSH1-3, which eluted at 4.03, 4.27 and 4.36 min (Figure 2A), respectively, were detected in all experiments. In the chemical stability experiments where compounds were incubated in GSH-supplemented phosphate buffer or in the presence of heat-inactivated liver S9 (rat and human), compound **1** was converted to the three conjugates at a low level (≤ 3%) (Figure 2B). When incubated with human liver microsomes (fortified with GSH alone or both GSH and NADPH) or human liver cytosol (with GSH), the yield of these conjugates of **1** was comparable on a cumulative basis (4 – 5%; Figure 2D and 2F). In contrast, when **1** was incubated with GSH-fortified rat liver preparations, the yield of the GSH conjugates rose 2- to 3-fold in microsomes, with or

without NADPH, and 16-fold in cytosol relative to that obtained following the reaction in heat-treated liver S9 or in buffer (Figure 2C and 2E). GSH1-3 was the most abundant conjugate in all incubations based on UV peak areas. Mass spectrometric analysis of the conjugates is described in the next section.

Compound **2** also reacted chemically with GSH, giving rise to multiple minor GSH adducts (P + 307 u) in both the potassium phosphate buffer and heat-inactivated liver S9 (human and rat). By comparison, larger amounts of these GSH adducts were formed in incubations with human (3-fold) or rat liver microsomes (9-fold) supplemented with GSH or both GSH and NADPH. When **2** was incubated with GSH-supplemented liver cytosol, still greater amounts of conjugates were observed in human (16-fold) and rat (56-fold). Four GSH conjugates, GSH2-1, GSH2-2, GSH2-3 and GSH2-4, were observed in all incubations based on their HPLC retention times (5.06, 5.18, 5.49 and 5.75 min, respectively; Figure 3A) and mass spectra. Specifically, GSH2-3 and GSH2-4 were the main adducts detected in rat liver microsomes and cytosol (Figure 3C and 3E) and in enzyme-free incubations (Figure 3B), whereas GSH2-1 and GSH2-4 were more abundant in human liver microsomes and cytosol (Figure 3D and 3F).

Compound **3** reacted to form a single GSH conjugate in buffer, although turnover was limited, and the conjugate was only detected by mass spectrometry. The amount of this conjugate formed in GSH-fortified incubations with liver microsomes (rat and human) and liver cytosol (human) was also lower than 1%. However, GSH-supplemented rat liver cytosol catalyzed the formation of this conjugate to a greater extent, resulting in a 7% yield.

As a general observation, the addition of NADPH to liver microsomes did not increase the yield of GSH conjugates of **1**, **2** and **3**. Also, greater amounts of conjugates were formed in rat liver preparations than in human liver preparations, and yields were higher in cytosol incubations than in microsomal incubations.

Compounds **4 – 8** did not form any GSH conjugates in any of the GSH-supplemented incubations.

Mass spectrometry of substrates The MS/MS product-ion spectrum of the protonated **1** (*m/z* 361) showed that fragmentation occurred on the oxazolidinone moiety, with losses of NHCO (43 u) and carbamic acid (61 u) giving rise to ions of *m/z* 318 and 300, respectively (Figure 4A). The base peak ion of *m/z* 209 and neighboring ions of *m/z* 195 and 182 were derived from losses of the fluorophenyl group and portions of the oxazolidinone as illustrated in the figure. Compounds **2** and **3** exhibited similar MS/MS fragmentation patterns to **1** (data not shown).

Mass spectrometry of GSH conjugates Each GSH conjugate of **1**, **2** and **3** formed a protonated molecule $[M+H]^+$ during positive-ion electrospray whose mass-to-charge ratio (*m/z*) was greater than that of the respective parent compound by *m/z* 307. The added group (307 u) exhibited the molecular weight of GSH, suggesting that the GSH group was added through addition to an unsaturated bond rather than through substitution, which would have resulted in a net molecular weight increase of 305 u.

The three GSH adducts (GSH1-1, GSH1-2 and GSH1-3) of **1** were detected by mass spectrometry and UV and also resolved as shown in HPLC chromatograms (Figure 2). The MS/MS product-ion spectrum of GSH1-3 (*m/z* 668), the most abundant GSH conjugate, formed product ions of *m/z* 593 and 539 corresponding to the characteristic

neutral loss of a 75 u (glycine) and 129 u (γ-glutamyl group), respectively, from the GSH moiety (Figure 4B). The product ion of *m/z* 393 and its neighboring ion of *m/z* 395 were produced by loss of 275 u and 273 u, respectively, from cleavage of the cysteinyl C-S bond. The product ions of *m/z* 539 and 393 fragmented further, by loss of CO_2 (44 u), to give rise to the ions of *m/z* 495 and 349, respectively. The product-ion mass spectrum of GSH1-3 was very similar to those of GSH1-1 and GSH1-2 (data not shown).

The four GSH adducts of **2** (GSH1-1, GSH2-2, GSH2-3 and GSH2-4) were well resolved as shown in the HPLC/UV chromatograms (Figure 3). The product-ion MS/MS spectrum of GSH2-3 (*m/z* 685) exhibited peaks of *m/z* 610 and 556, resulting from neutral losses of 75 u and 129 u, respectively (Figure 5). Loss of 273 u and 275 u via cleavage of the cysteinyl C-S bond gave rise to the product ions of *m/z* 412 and *m/z* 410, respectively. Consecutive losses of CO_2 and HF (20 u) from the ion of *m/z* 412 gave rise to the product ions of *m/z* 368 and 348, respectively. Product-ion MS/MS spectra of GSH2-1 and GSH2-4 (data not shown) exhibited similar fragmentation patterns to that of GSH2-3. Due to the low level of GSH2-2 formed in all incubations, the product ion spectrum only showed fragments derived from neutral losses of 75 u, 129 u and 273 u (data not shown).

The only GSH adduct of compound **3**, GSH3-1, formed a protonated molecule of *m/z* 703 during positive-ion electrospray mass spectrometry. Following collision-induced dissociation (CID), GSH3-1 gave rise to multiple product ions of *m/z* 628, 574, 557, 471 and 430, resulting from neutral loss of 75 u, 129 u, 146 u (129 + NH_3), 232 u (129 + 75 + CO) and 273 u, respectively (Figure 6). The ion of *m/z* 430 fragmented further via the loss of formic acid (46 u) from the oxazolidinone to yield the product ion of *m/z* 384.

Additionally, the product ions of *m/z* 574 and *m/z* 471 fragmented further by the loss of carbamic acid from the oxazolidinone moiety, giving rise to product ions of *m/z* 513, and 410, respectively.

The product ions of *m/z* 199 and 155 were observed in the mass spectra of all conjugates, except in that of GSH2-2. The ion of *m/z* 199 was formed by cleavage of the cysteinyl C–S bond and neutral losses of glycine, and the ion of *m/z* 155 resulted from additional loss of CO_2 from this GSH-derived fragment ion.

NMR Spectroscopy The ^{1}H and ^{13}C chemical shifts of **1** and **2**, as well as those of their isolated GSH conjugates (GSH1-2, GSH1-3, GSH2-3 and GSH2-4), were obtained from ^{1}H NMR spectra and HMQC spectra, respectively. The ^{13}C NMR spectra of **1** and **2** were also recorded. The chemical shifts of **1** and associated GSH conjugates are summarized in Table 2, and the chemical shifts of **2** and its GSH conjugates are summarized in Table 3. The protons of the aromatic rings, including the fluorophenyl, the two heteroaryls flanking the acetylene, and those of the oxazolidinone moiety in the parent compounds and their respective GSH conjugates, were characterized by minor differences in chemical shifts.

The ^{1}H NMR spectrum of GSH1-3 indicated the presence of an extra singlet proton of 7.01 ppm, which correlated to a new ^{13}C resonance of 127.7 ppm by HMQC, a characteristic chemical shift for an alkene. The HMBC experiment revealed long-range C-H correlations between the extra proton and both C16 and C23 (Figure 7). The ROESY spectrum of GSH1-3 revealed through-space interactions between the extra proton and both H15 and H17 (Figure 8), indicating proximity to the paired protons.

In comparison to the NMR spectra of **1**, one- and two-dimensional NMR spectra of GSH1-2 revealed an extra proton of 7.60 ppm, which correlated to a new alkene ^{13}C signal of 134.2 ppm. However, the amount of the isolated GSH1-2 was insufficient to allow additional HMBC and ROSEY experiments to be performed.

Similarly, GSH2-3 and GSH2-4 exhibited extra protons of 7.15 ppm (GSH2-3) or 6.84 ppm (GSH2-4) and corresponding correlations with new ethylene ^{13}C signals of either 121.9 ppm (GSH2-3) or 128.8 ppm (GSH2-4). A long-range C-H correlation study (HMBC) revealed connectivity between C14 and the extra proton of GSH2-3 (Figure 9). Moreover, the through-space interaction between the extra proton and the pyridine proton H15 of GSH2-3 was also observed (Figure 10). HMBC and ROSEY spectra of GSH2-4 were not obtained due to the limited amount of the product that was isolated.

Discussion

Multiple GSH conjugates of **1** and **2** were formed in the present study, each exhibiting a shift in molecular weight of 307 u compared with its respective parent compound. Such a shift typically marks a loss of one double-bond equivalent during the biotransformation sequence and indicates that a reaction has proceeded by addition. The MS/MS fragmentation of the cysteinyl C-S bond gave rise to product ions by shedding 273 u, with or without the loss of two additional hydrogens, in all GSH conjugates. Furthermore, no product ions were formed that might have signaled the loss of the whole GSH moiety. These mass spectrometric findings provided further evidence that the GSH group was connected via a non-sp^3-hybridized carbon, excluding the possibility of connection of the GSH moiety to carbons 2 or 3 of the oxazolidinone ring (refer to Tables

2 and 3 for atom numbering). The major MS/MS product ions of these conjugates were formed by cleavages involving portions of the GSH moiety. However, interpretation and comparison of the fragmentation patterns of the parents and the GSH conjugates did not allow the sites of GSH conjugation to be defined regiochemically, specifically with respect to the question of whether the GSH moieties were attached to the aromatic carbons or, alternatively, the acetylene groups.

NMR spectra of the four isolated conjugates unambiguously demonstrated the presence of a newly added proton in each metabolite that was connected to a newly formed double bond. Additionally, the aromatic protons that were present in the substrates were fully accounted for and had remained intact (Tables 2 and 3). Taken together, the LC-MS and NMR results indicated that GSH conjugation had involved conversion of the acetylene moiety to a double bond. Furthermore, the through-bond correlation (HMBC) between the newly formed vinyl protons and carbons of the neighboring aromatic moieties (C16 and C23 in GSH1-3; C14 in GSH2-3) allowed regiochemical assignment of the proton as being bound to C21, and GSH moiety to C20, in both conjugates (Figures 7 and 9). The ROSEY results of GSH1-3 revealed through-space proximity between the vinyl proton (H21) and H15/H17 due to free rotation of the bond connecting C20 and C16, demonstrating the double bond geometry to be *Z* (Figure 8). Likewise, the ROESY spectrum was also used to assign the same configuration to the double bond of GSH2-3 based on a correlation between H21 and H15 (Figure 10). The remaining conjugates of **1** and **2** were tentatively proposed to represent the corresponding configurational isomers or regioisomers of GSH1-3 and GSH2-3, respectively (refer to Figure 11 for the four isomeric GSH conjugates of compound **2** as an example), although

the low abundances of these metabolites precluded the acquisition of their 2D NMR spectra. The sole GSH conjugate of **3** was also proposed to form across the acetylene moiety.

GSH addition to the acetylene groups of **1**, **2** and **3** was observed in the absence of active liver microsomes or cytosol, suggesting that the acetylene moieties of these compounds were electrophilic enough to react spontaneously with a nucleophilic thiolate anion (GS^-). The thiolate in aqueous solution (pH 7.4) is expected to represent $< 2.5\%$ of total GSH content based on its pKa of 9 (Tang and Chang, 1996). Additionally, supplementation of NADPH to microsomal incubations did not enhance the formation of GSH conjugates (P + 307 u) compared with microsomal incubations that lacked NADPH, indicating that P450 was not involved in catalysis. The reaction with GSH was enhanced greatly in liver cytosol and to a lesser extent in liver microsomes, suggesting the catalytic contribution of GSTs. These enzymes are known to catalyze such reactions by creating a local environment where the pKa of GSH is lowered to approximately 6.8 under physiological conditions, producing the thiolate anion which is stabilized by hydrogen bonding in the active site. This process increases the content of GS^- to 80% and facilitates subsequent nucleophilic attack onto an electrophile docked in a second substrate binding site (Graminski et al., 1989; Tang and Chang, 1996). Therefore, one might speculate that increasing the pH of the incubation buffer might also serve as a means of boosting conjugate formation.

Microsomal and cytosolic GSTs both utilize the stabilized nucleophilic thiolate anion to conjugate with foreign or endogenous electrophiles as a fundamental aspect of catalysis. While there is little homology in the amino acid sequences of the two groups of

GSTs (Commandeur et al., 1995), these differences were not manifest in terms of differing substrate specificity or regio- and stereo-selectivity of product formation with respect to the mGluR5 PAMs evaluated in this study. Indeed, the product profiles that were observed following microsomal and cytosolic metabolism were qualitatively similar. However, liver cytosol has been documented to exhibit more than 10 times greater catalytic activity than liver microsomes, and low sequence homology between rat and human enzymes (> 40% within the same class and < 25% across classes) is believed to affect substrate specificity and enzyme kinetics (Commandeur et al., 1995; Hayes et al., 2005). This difference was especially evident in the rat, where cytosolic GSTs were more active toward **1**, **2** and **3** than their microsomal counterparts. The difference in performance between the human liver fractions was smaller, especially for **1** and **3**. Moreover, in all cases, metabolic turnover was markedly higher in rat cytosol relative to human cytosol, and marginally higher in rat microsomes than in human microsomes. Therefore, the results suggested species-related differences between microsomal and cytosolic GSTs in terms of their catalytic efficiency toward these mGluR5 PAMs.

Interestingly, **4 – 8** were unreactive toward GSH in all incubations despite their structural similarity to **1**, **2**, and **3**. This disparity appears to be driven by proximity of the acetylene to neighboring heteroaryl rings. The heteroarenes enhance the electrophilic character of the acetylene via electron-withdrawing effects and explain why acetylenes that are flanked by two heteroaryl rings (**1**, **2**, **3**) are more prone to the formation of GSH conjugates than compounds bearing either one heteroaryl and one phenyl ring (**4**, **5**, **6**), one heteroaryl and one cyclohexyl ring (**8**), or phenyl rings only (**7**), any of which would exhibit lower electrophilicity as a result of increased electron density about the triple

bond. There are precedents in the literature for the influence of electronic factors in this way. For example, the internal acetylene of efavirenz did not undergo GSH conjugation, whereas its metabolite, which featured an electron-withdrawing hydroxyl group on the carbon adjacent to the triple bond, did form such conjugates (Mutlib et al., 1999a). The enhanced susceptibility of **1** and **2** to GSH conjugation can be further explained by the positions of the pyridine or pyrazine nitrogen atoms in their respective heteroaryl rings. During nucleophilic addition, the developing negative charge can be delocalized through resonance onto the aryl nitrogen atoms of **1** and **2**, as illustrated in Figure 11, resulting in lowered energy of activation. While **3 – 8** allow delocalization of the negative charge through resonance, none of the canonical resonance structures places the negative charge onto nitrogen.

GSH conjugation often represents a detoxification pathway of electrophilic xenobiotics, their oxidized intermediates, and by-products of oxidative stress, protecting cellular proteins and nucleic acids from damage or mutation. On the other hand, GSH conjugates of certain compounds can trigger downstream toxicological events through covalent modification of cellular macromolecules and / or transport of reversibly bound electrophiles followed by dissociation and concentration at a remote site. It remains unknown whether the GSH conjugates reported in the present study represent any such risk. As an alternative consequence of GSH-dependent processes, extensive GSH conjugation achieved using a high dose of a reactive compound may decrease the physiological level of GSH, especially in subjects whose GSH content has been lowered by excess alcohol consumption or disease states (e.g. HIV infection and tuberculosis), leading to compromised defenses against hepatotoxicity (Herzenberg et al., 1997; Chan et

al., 2001; Morris et al., 2013). The metabolite profiling results of **1** and **2** prompted concern that these compounds might carry the latter liability. Therefore, the observation that GSH conjugation could be avoided by flanking the triple bond with only one electron-withdrawing aryl ring was an insight that helped drive the structural optimization of the mGluR5 PAM series during drug discovery. In addition, placing the acetylene at the C3 position of the pyridines prevented delocalization of the negative charge onto the nitrogen

In summary, we demonstrated that mGluR5 PAMs featuring biheteroaryl acetylenes formed GSH conjugates both nonenzymatically and via catalysis by GSTs. The extent of GSH-conjugate formation in liver fractions was subject to species-related differences in the catalytic efficiency of the relevant GSTs. More importantly, the reactivity of the acetylene groups of these compounds appeared to depend on the structures of adjacent aryl functional groups, and the structure-property relationships that were revealed helped identify the acetylene flanked by two heteroaryl rings as a potentially problematic feature. Pursuant to this discovery, biheteroaryl acetylenes were excluded from this series of mGluR5 PAMs in the interest of identifying a development candidate with an acceptable safety profile.

Authorship Contribution

Participated in research design: Zhuo, Johnson, X. S. Huang

Conducted experiments: Zhuo, X. S. Huang

Contributed new agents or analytical tools: Degnan, Snyder, Yang, H. Huang

Performed data analysis: Zhuo, X. S. Huang, Johnson

Wrote or contributed to the writing of the manuscript: Zhuo, Johnson, Degnan, X. S. Huang, Shu

References

Awad H, Hubert GW, Smith Y, Levey AI, and Conn PJ (2000) Activation of metabotropic glutamate receptor 5 has direct excitatory effects and potentiates NMDA receptor currents in neurons of the subthalamic nucleus. *J Neurosci* **20:**7871-7879.

Chan K, Han XD, and Kan YW (2001) An important function of Nrf2 in combating oxidative stress: detoxification of acetaminophen. *Proc Natl Acad Sci U S A* **98:**4611-4616.

Chen H, Shockcor J, Chen W, Espina R, Gan LS, and Mutlib AE (2002) Delineating novel metabolic pathways of DPC 963, a non-nucleoside reverse transcriptase inhibitor, in rats. Characterization of glutathione conjugates of postulated oxirene and benzoquinone imine intermediates by LC/MS and LC/NMR. *Chem Res Toxicol* **15:**388-399.

Commandeur JN, Stijntjes GJ, and Vermeulen NP (1995) Enzymes and transport systems involved in the formation and disposition of glutathione S-conjugates. Role in bioactivation and detoxication mechanisms of xenobiotics. *Pharmacol Rev* **47:**271-330.

Conn PJ, Lindsley CW, and Jones CK (2009) Activation of metabotropic glutamate receptors as a novel approach for the treatment of schizophrenia. *Trends Pharmacol Sci* **30:**25-31.

Graminski GF, Kubo Y, and Armstrong RN (1989) Spectroscopic and kinetic evidence for the thiolate anion of glutathione at the active site of glutathione S-transferase. *Biochemistry* **28:**3562-3568.

Hayes JD, Flanagan JU, and Jowsey IR (2005) Glutathione transferases. *Annu Rev Pharmacol Toxicol* **45:**51-88.

Herzenberg LA, De Rosa SC, Dubs JG, Roederer M, Anderson MT, Ela SW, Deresinski SC, and Herzenberg LA (1997) Glutathione deficiency is associated with impaired survival in HIV disease. *Proc Natl Acad Sci U S A* **94:**1967-1972.

Iverson SL and Uetrecht JP (2001) Identification of a reactive metabolite of terbinafine: insights into terbinafine-induced hepatotoxicity. *Chem Res Toxicol* **14:**175-181.

Kalgutkar AS, Gardner I, Obach RS, Shaffer CL, Callegari E, Henne KR, Mutlib AE, Dalvie DK, Lee JS, Nakai Y, O'Donnell JP, Boer J, and Harriman SP (2005) A comprehensive listing of bioactivation pathways of organic functional groups. *Curr Drug Metab* **6:**161-225.

Kinney GG, Burno M, Campbell UC, Hernandez LM, Rodriguez D, Bristow LJ, and Conn PJ (2003) Metabotropic glutamate subtype 5 receptors modulate locomotor activity and sensorimotor gating in rodents. *J Pharmacol Exp Ther* **306:**116-123.

Lindsley CW, Shipe WD, Wolkenberg SE, Theberge CR, Williams DL, Jr., Sur C, and Kinney GG (2006) Progress towards validating the NMDA receptor hypofunction hypothesis of schizophrenia. *Curr Top Med Chem* **6:**771-785.

Liu F, Grauer S, Kelley C, Navarra R, Graf R, Zhang G, Atkinson PJ, Popiolek M, Wantuch C, Khawaja X, Smith D, Olsen M, Kouranova E, Lai M, Pruthi F, Pulicicchio C, Day M, Gilbert A, Pausch MH, Brandon NJ, Beyer CE, Comery TA, Logue S, Rosenzweig-Lipson S, and Marquis KL (2008) ADX47273 [S-(4-fluoro-phenyl)-{3-[3-(4-fluoro-phenyl)-[1,2,4]-oxadiazol-5-yl]-piperidin-1- yl}-methanone]: a novel metabotropic glutamate receptor 5-selective positive

allosteric modulator with preclinical antipsychotic-like and procognitive activities. *J Pharmacol Exp Ther* **327:**827-839.

Marino MJ and Conn PJ (2002) Modulation of the basal ganglia by metabotropic glutamate receptors: potential for novel therapeutics. *Curr Drug Targets CNS Neurol Disord* **1:**239-250.

Morris D, Khurasany M, Nguyen T, Kim J, Guilford F, Mehta R, Gray D, Saviola B, and Venketaraman V (2013) Glutathione and infection. *Biochim Biophys Acta* **1830:**3329-3349.

Mutlib AE, Chen H, Nemeth G, Gan LS, and Christ DD (1999a) Liquid chromatography/mass spectrometry and high-field nuclear magnetic resonance characterization of novel mixed diconjugates of the non-nucleoside human immunodeficiency virus-1 reverse transcriptase inhibitor, efavirenz. *Drug Metab Dispos* **27:**1045-1056.

Mutlib AE, Chen H, Nemeth GA, Markwalder JA, Seitz SP, Gan LS, and Christ DD (1999b) Identification and characterization of efavirenz metabolites by liquid chromatography/mass spectrometry and high field NMR: species differences in the metabolism of efavirenz. *Drug Metab Dispos* **27:**1319-1333.

Ortiz de Montellano PR (2005) *Cytochrome P450-Structure, Mechanism, and Biochemistry*. Luwer Academic/Plenum Publishers, New York.

Perroy J, Raynaud F, Homburger V, Rousset MC, Telley L, Bockaert J, and Fagni L (2008) Direct interaction enables cross-talk between ionotropic and group I metabotropic glutamate receptors. *J Biol Chem* **283:**6799-6805.

Pisani A, Gubellini P, Bonsi P, Conquet F, Picconi B, Centonze D, Bernardi G, and Calabresi P (2001) Metabotropic glutamate receptor 5 mediates the potentiation of N-methyl-D-aspartate responses in medium spiny striatal neurons. *Neuroscience* **106:**579-587.

Tang SS and Chang GG (1996) Kinetic characterization of the endogenous glutathione transferase activity of octopus lens S-crystallin. *Journal of biochemistry* **119:**1182-1188.

Tomigahara Y, Shiba K, Isobe N, Kaneko H, Nakatsuka I, and Yamada H (1994) Identification of two new types of S-linked conjugates of Etoc in rat. *Xenobiotica* **24:**839-852.

Figure legend

Figure 1 Structures of eight mGluR5 PAMs

Figure 2 Positive-ion electrospray LC-MS extracted ion chromatogram (*m/z* 668) illustrating the elution of GSH conjugates (GSH1-1, GSH1-2 and GSH1-3) of **1** (A). HPLC-UV chromatograms of **1** and its GSH conjugates detected in GSH-fortified incubations without liver subcellular preparations (B), with rat liver microsomes (RLM) (C), human liver microsomes (HLM) (D), rat liver cytosol (RLC) (E), and human liver cytosol (HLC) (F).

Figure 3 Positive-ion electrospray LC-MS extracted ion chromatogram (*m/z* 685) showing the elution of GSH conjugates (GSH2-1, GSH2-2, GSH2-3 and GSH2-4) of **2** (A). HPLC-UV chromatograms of **2** and its GSH conjugates detected in GSH-fortified incubations without liver subcellular preparations (B), with rat liver microsomes (RLM) (C), human liver microsomes (HLM) (D), rat liver cytosol (RLC) (E), and human liver cytosol (HLC) (F).

Figure 4 Product-ion MS/MS spectra of **1** (panel A) and GSH1-3 (panel B) annotated with proposed structures of fragment ions.

Figure 5 Product ion MS/MS spectrum of GSH2-3 and proposed structures of fragment ions

Figure 6 Product ion MS/MS spectrum of GSH3-1 and proposed structures of fragment ions

Figure 7 Heteronuclear multiple bond correlation (HMBC) spectrum of GSH1-3, which was isolated from an incubation of **1** with GSH-fortified Aroclor-induced rat liver S9

Figure 8 Rotating frame Overhauser enhancement spectroscopy (ROSEY) spectrum of GSH1-3, which was isolated from an incubation of **1** with GSH-fortified Aroclor-induced rat liver S9

Figure 9 Heteronuclear multiple bond correlation (HMBC) spectrum of GSH2-3, which was isolated from an incubation of **2** with GSH-fortified Aroclor-induced rat liver S9

Figure 10 Rotating frame Overhauser enhancement spectroscopy (ROSEY) spectrum of GSH2-3, which was isolated from an incubation of **2** with GSH-fortified Aroclor-induced rat liver S9

Figure 11 A proposed mechanism of GSH addition to the acetylene of **2**. The thiolate anion (GS^-), formed either spontaneously or as a result of catalysis by GST, initiates nucelophilic attack on either acetylenic carbon atom to produce four isomeric GSH conjugates. The negatively charged intermediate is stabilized by the nitrogen atoms of the heteroaryl rings adjacent to the triple bond. The structure and stereochemistry of GSH2-3

was confirmed by LC/MS and NMR results, and the conjugates GSH2-1, GSH2-2, and GSH2-4 were proposed as isomers.

DMD Fast Forward. Published on January 29, 2015 as DOI: 10.1124/dmd.114.061879
This article has not been copyedited and formatted. The final version may differ from this version.

TABLE 1 Each numerical entry represents the relative abundance (%) of all GSH conjugates combined that were formed via conjugate addition during the reaction of the compound listed at left. The values were estimated based on the ratio of UV peak areas of the GSH conjugates detected following a 30-min incubation to that of the respective parent compound at 0 min. The values represent means of duplicate measurements for each incubation.

	Combined amount of GSH conjugates [% of the original parent drug level (10 μM)]								
Liver subcellular fractions or buffer	Potassium phosphate buffer	Heat-inactivated liver S9		Liver Microsomes				Liver Cytosol	
Species	NA [a]	H [b]	R [c]	H	H	R	R	H	R
Cofactor(s)	GSH	GSH	GSH	GSH + NADPH	GSH	GSH + NADPH	GSH	GSH	GSH
Compound **1**	2	3	3	4	4	6	10	5	48
Compound **2**	1	1	1	3	4	8	9	16	56
Compound **3**	MS [d]	MS	MS	MS	< 1	< 1	< 1	< 1	7
Compounds **4 - 8**	ND [e]	ND	ND	ND	ND	ND	ND	ND	ND

[a] Not applicable

[b] Human

[c] Rat

[d] detected only by mass spectrometry with no UV response

[e] Not detected

DMD Fast Forward. Published on January 29, 2015 as DOI: 10.1124/dmd.114.061879
This article has not been copyedited and formatted. The final version may differ from this version.

TABLE 2 Proton (^{1}H NMR) and carbon chemical shifts (^{13}C NMR for parent and HMQC for conjugates) of **1** and its two GSH conjugates (GSH1-2 and GSH1-3). The proposed structure of GSH1-3 (*Z*) is shown below. The numbering system is for illustrative purposes only and does not correspond to IUPAC nomenclature.

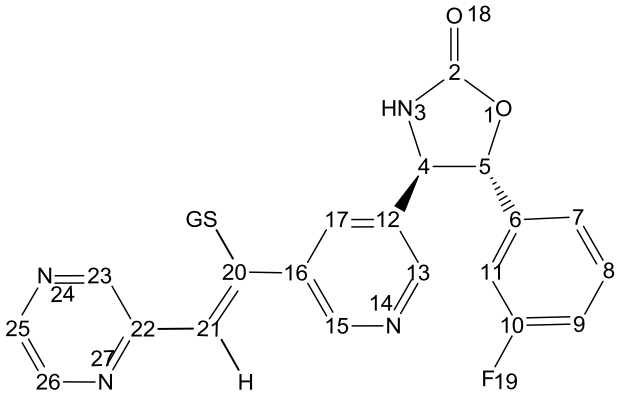

	δH ppm			δC ppm		
Position	**1**	GSH1-2	GSH1-3	**1**	GSH1-2	GSH1-3
3	8.52	ND [a]	ND			
4	5.00	4.95	5.00	60.9	61.8	61.7
5	5.54	5.45	5.50	82.8	83.2	83.1
7	7.24	7.26	7.23	122.6	123.4	122.9
8	7.44 – 7.58	7.55	7.45 – 7.55	132.0	131.8	131.6
9	7.26 – 7.37	7.26	7.25	116.9	116.6	116.4
11	7.26 – 7.37	7.30	7.35	113.6	113.8	113.6
13	8.59	8.38	8.47	148.9	147.7	148.6
15	8.86	8.87	8.72	140.2	151.0	140.2
17	8.14	8.23	7.94	138.5	138.2	134.5
20	NA [b]	7.60 [c]	NA	88.55	134.2 [c]	NA
21	NA		7.01	89.36		127.7

23	8.95	9.10	8.92	147.9	144.2	146.2
25	8.73	8.75	8.50	143.9	144.4	142.2
26	8.69	8.65	8.72	146.2	144.6	144.0

[a] Not detected

[b] Not applicable

[c] Site could not be assigned because HMBC and ROSEY spectra could not be acquired

DMD Fast Forward. Published on January 29, 2015 as DOI: 10.1124/dmd.114.061879
This article has not been copyedited and formatted. The final version may differ from this version.

TABLE 3 Proton (^{1}H NMR) and carbon chemical shifts (^{13}C NMR for parent and HMQC for conjugates) of **2** and its two GSH conjugates (GSH2-3 and GSH2-4). The proposed structure of GSH2-3 is shown below. The numbering system is for illustrative purposes only and does not correspond to IUPAC nomenclature.

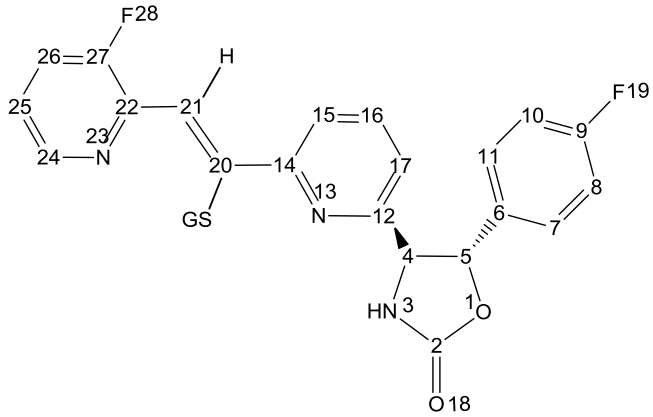

	δH ppm			δC ppm		
Position	**2**	GSH2-3	GSH2-4	**2**	GSH2-3	GSH2-4
3	8.59 – 8.47	8.54	8.53	NA	NA	NA
4	4.93	4.92	4.90	63.7	64.2	64.1
5	5.59	5.62	5.79	81.9	82.2	81.2
7	7.51	7.54	7.54	128.5	129.0	128.6
8	7.29	7.26	7.32	115.7	116.4	116.1
10	7.29	7.26	7.32	115.7	116.4	116.1
11	7.51	7.53	7.54	128.5	129.0	128.6
15	7.76	7.67	7.57	127.6	123.4	124.4
16	8.00	8.00	7.87	138.4	139.0	137.9
17	7.60 – 7.57	7.47	7.54	122.2	120.9	119.8
20	NA [a]	NA		81.9	NA	
21	NA	7.15	6.84 [b]	93.0	121.9	128.8 [b]
24	8.59 – 8.47	8.55	8.53	146.7	145.1	145.8

25	7.64 – 7.61	7.40	7.54	126.4	124.1	125.6
26	7.76	7.72	7.88	124.1	123.4	125.2

[a] Not applicable

[b] Site could not be assigned because HMBC and ROSEY spectra were unavailable

Figure 1

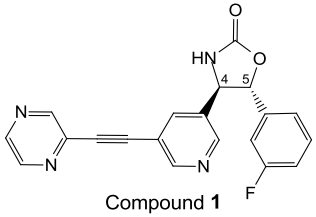

Compound **1**

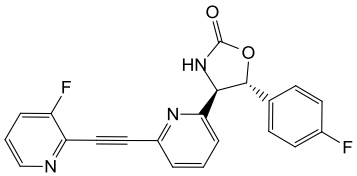

Compound **2**

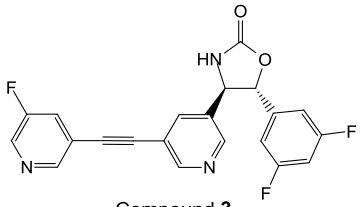

Compound **3**

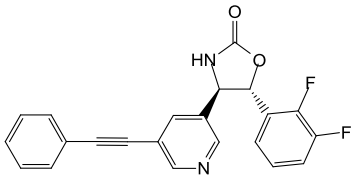

Compound **4**

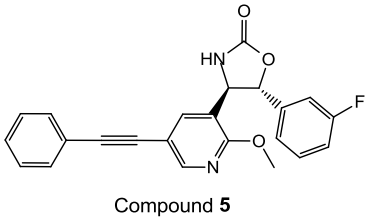

Compound **5**

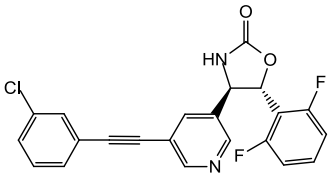

Compound **6**

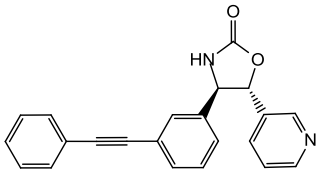

Compound **7**

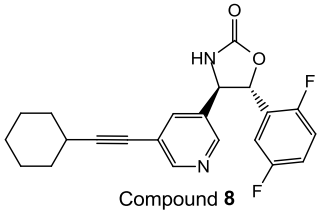

Compound **8**

Figure 2

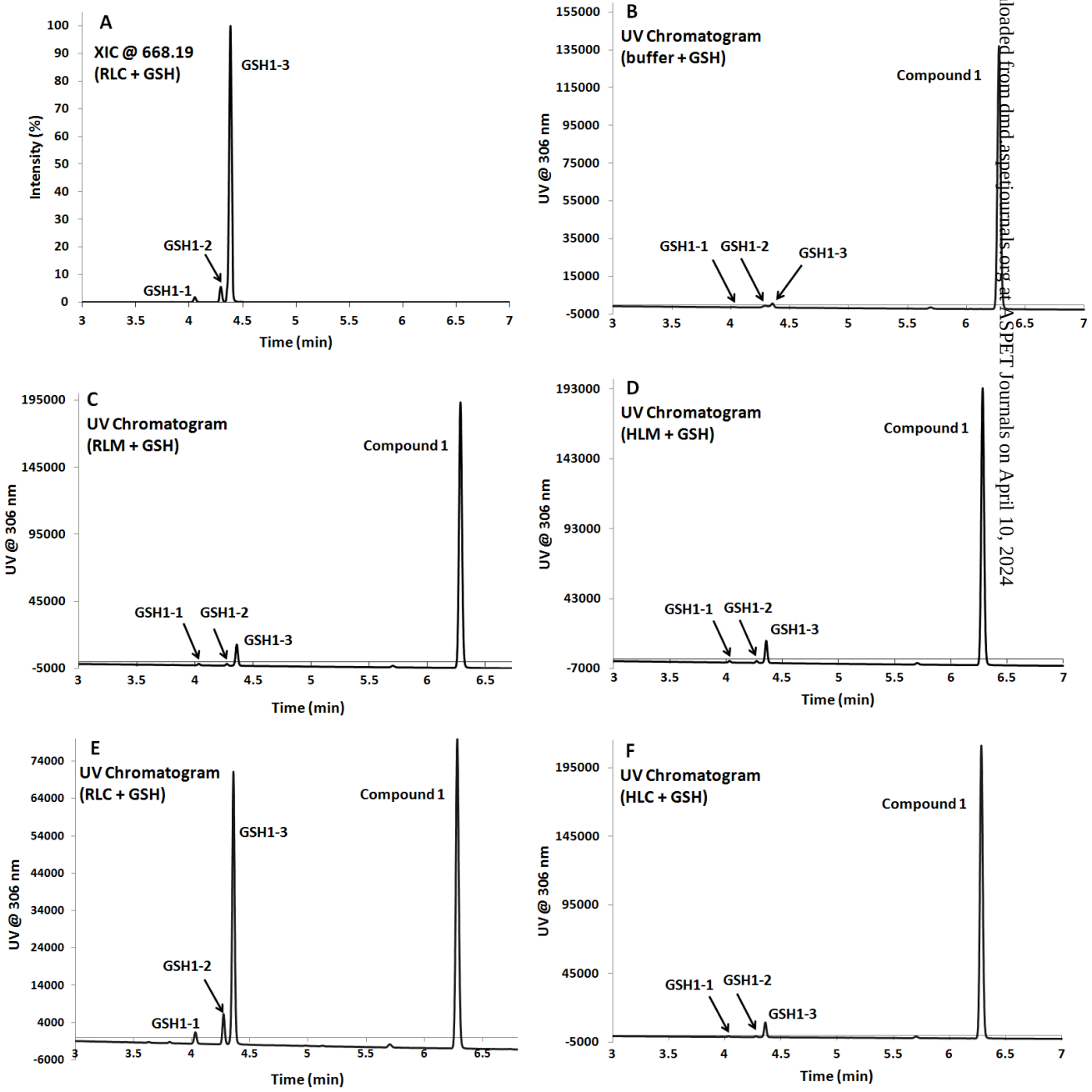

Figure 3

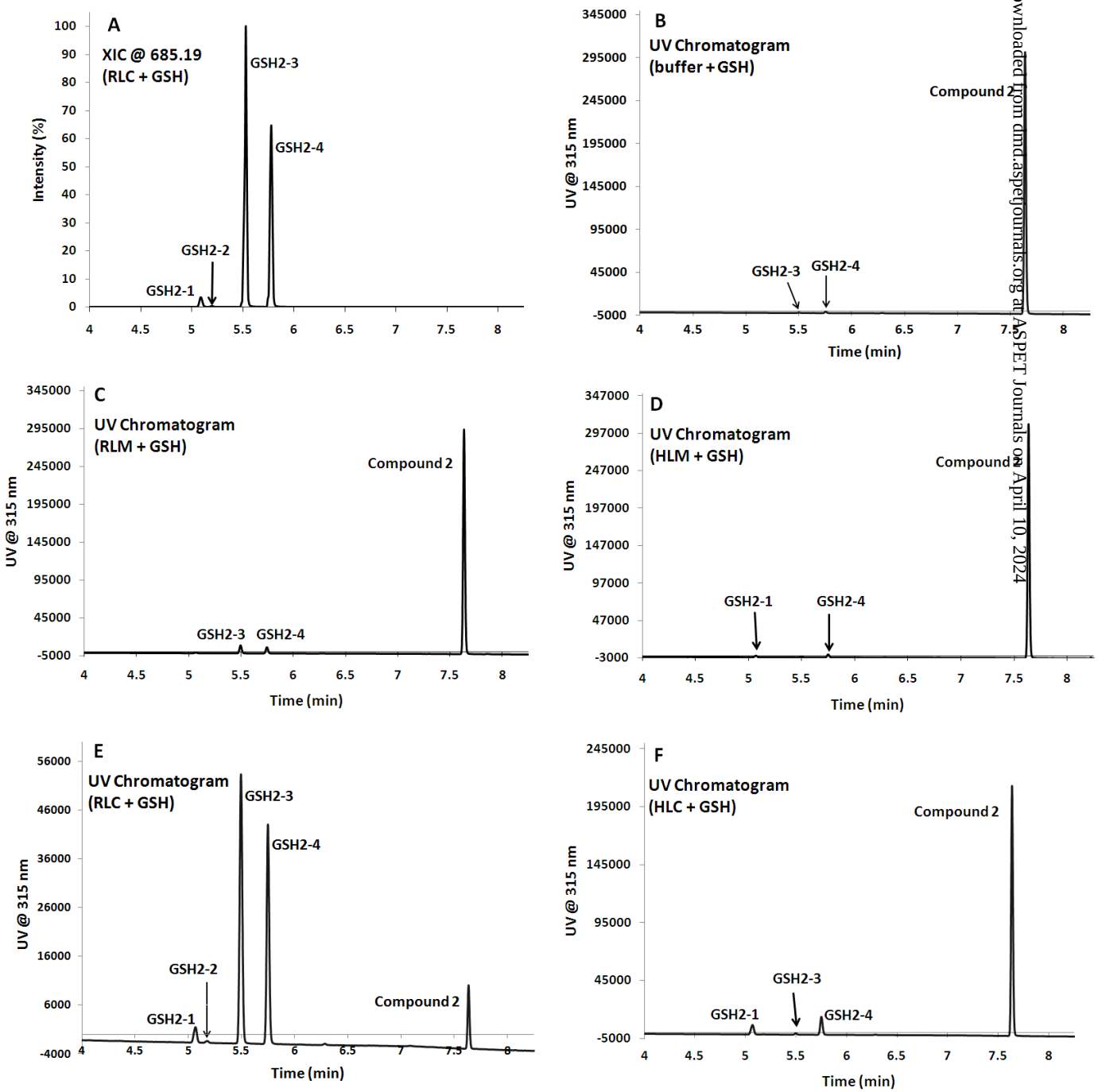

Figure 4A

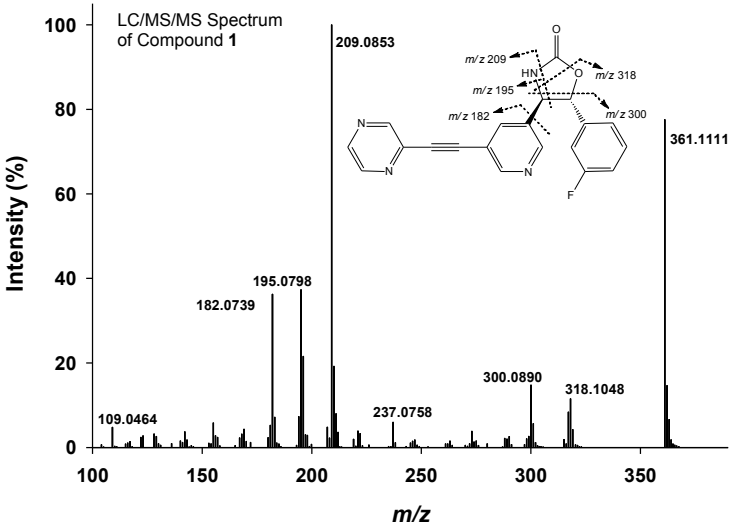

Figure 4B

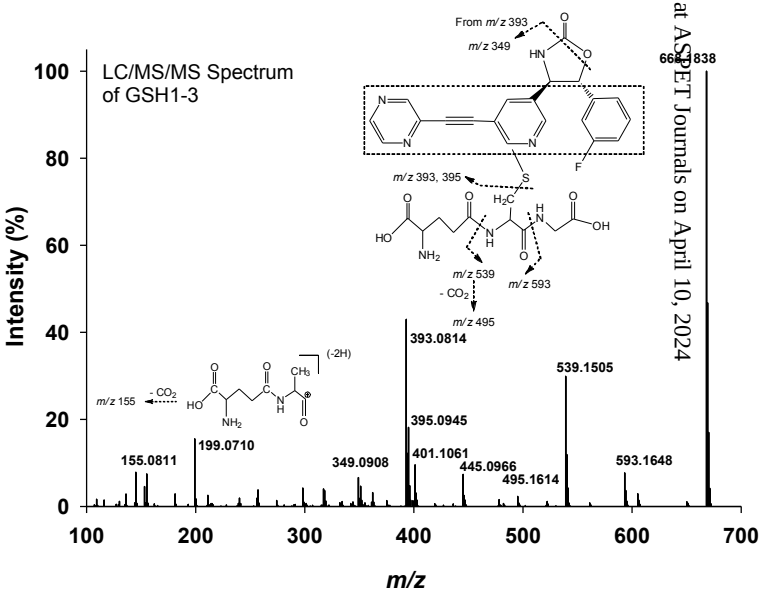

Figure 5

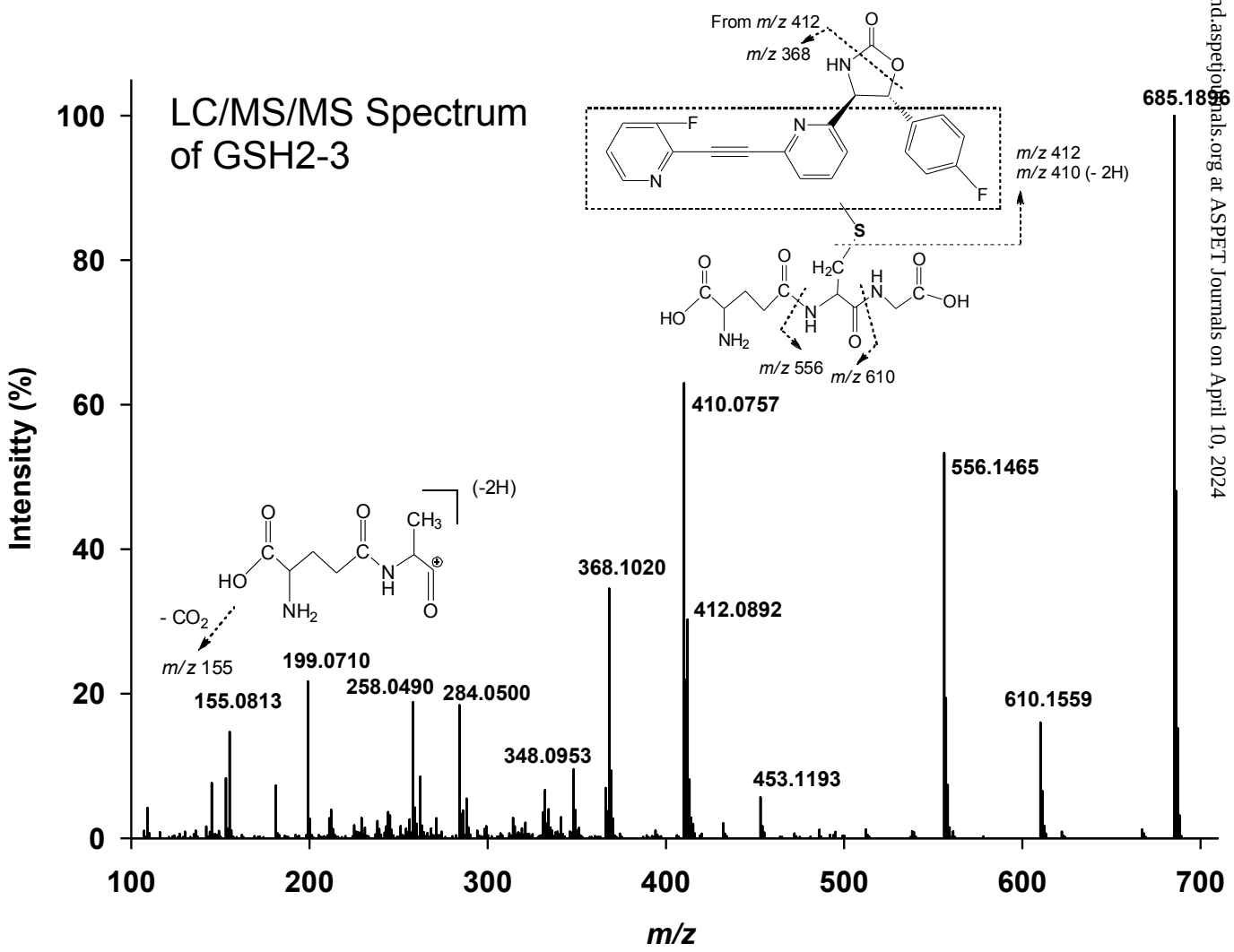

Figure 6

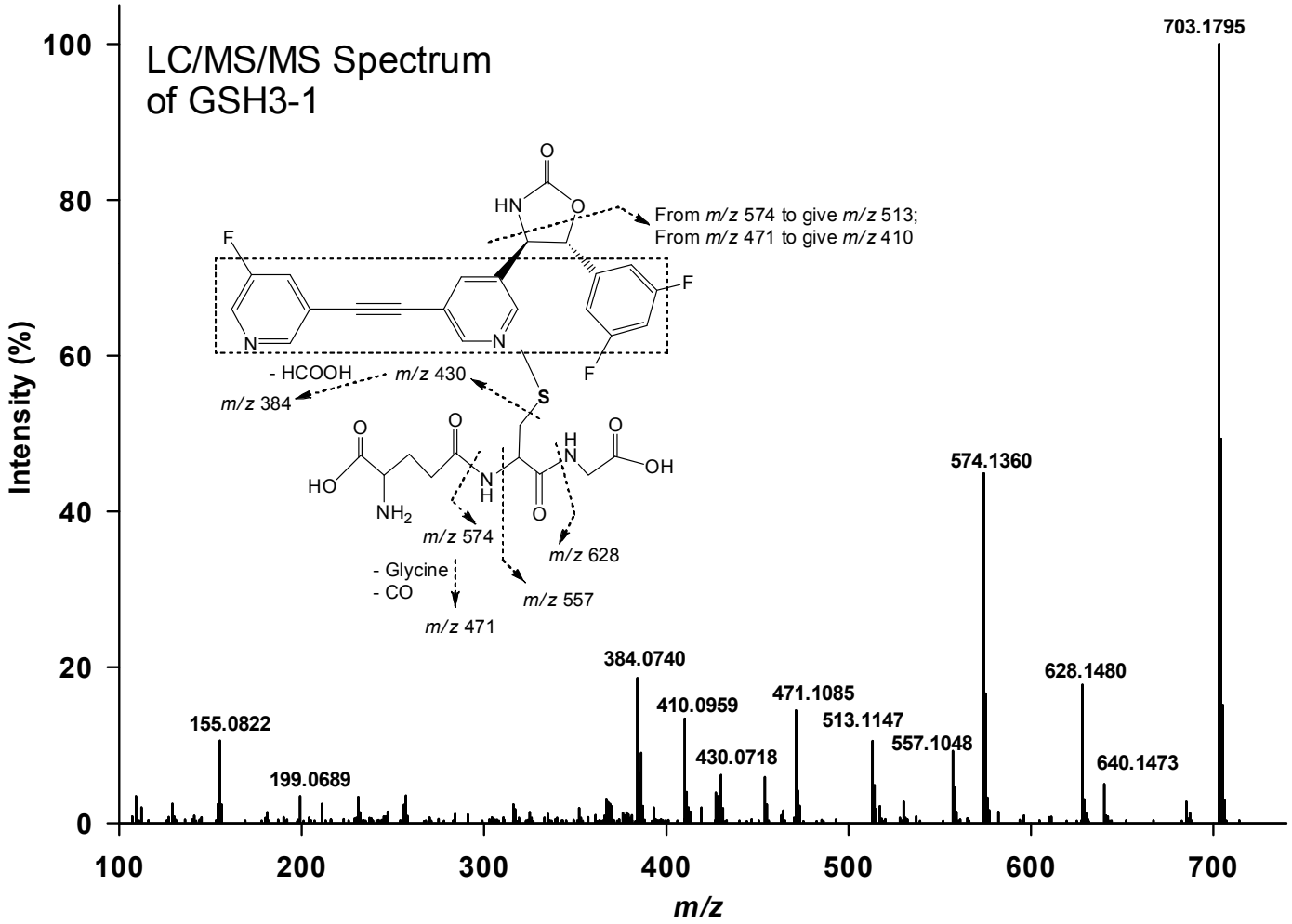

Figure 7

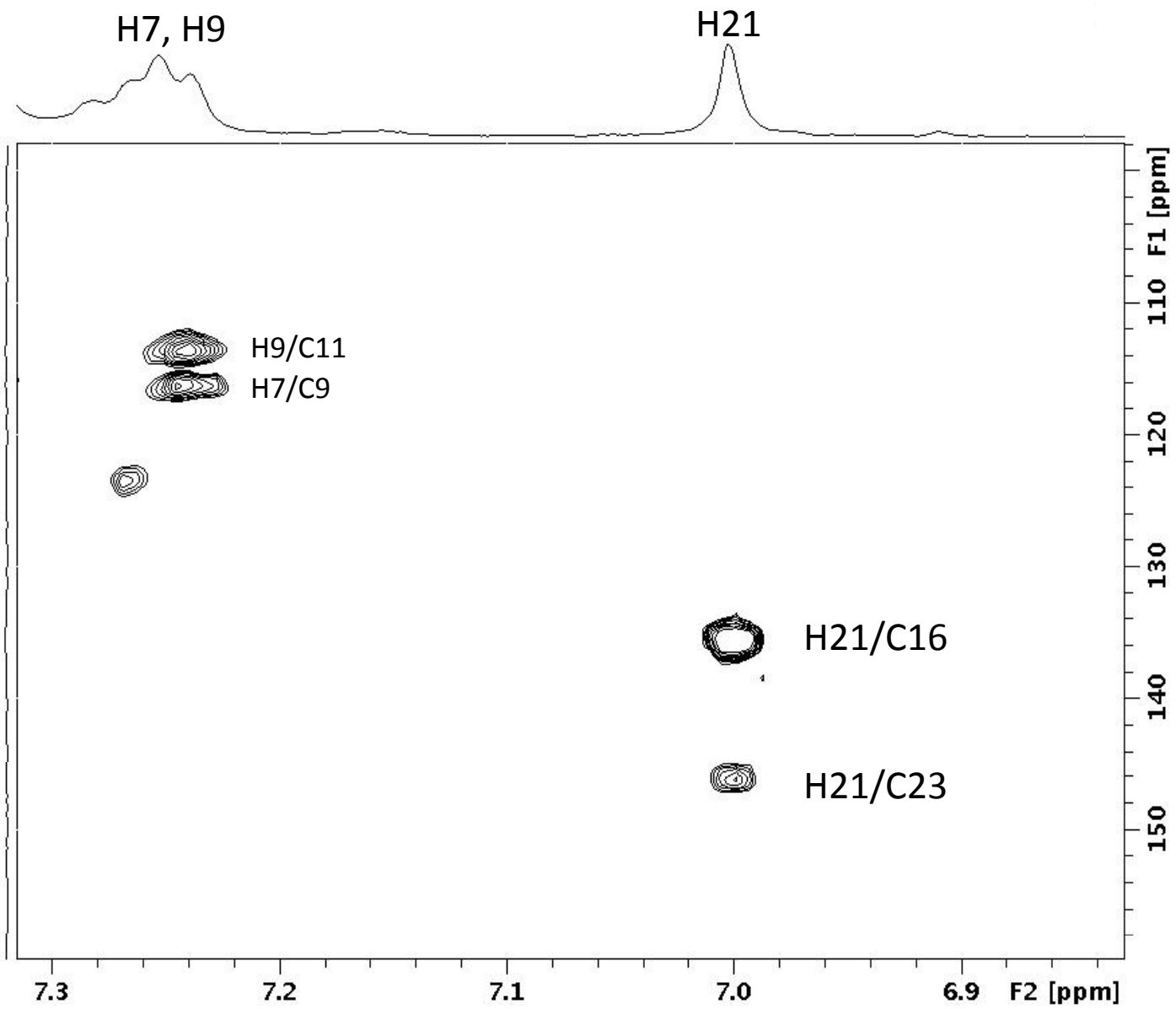

Figure 8

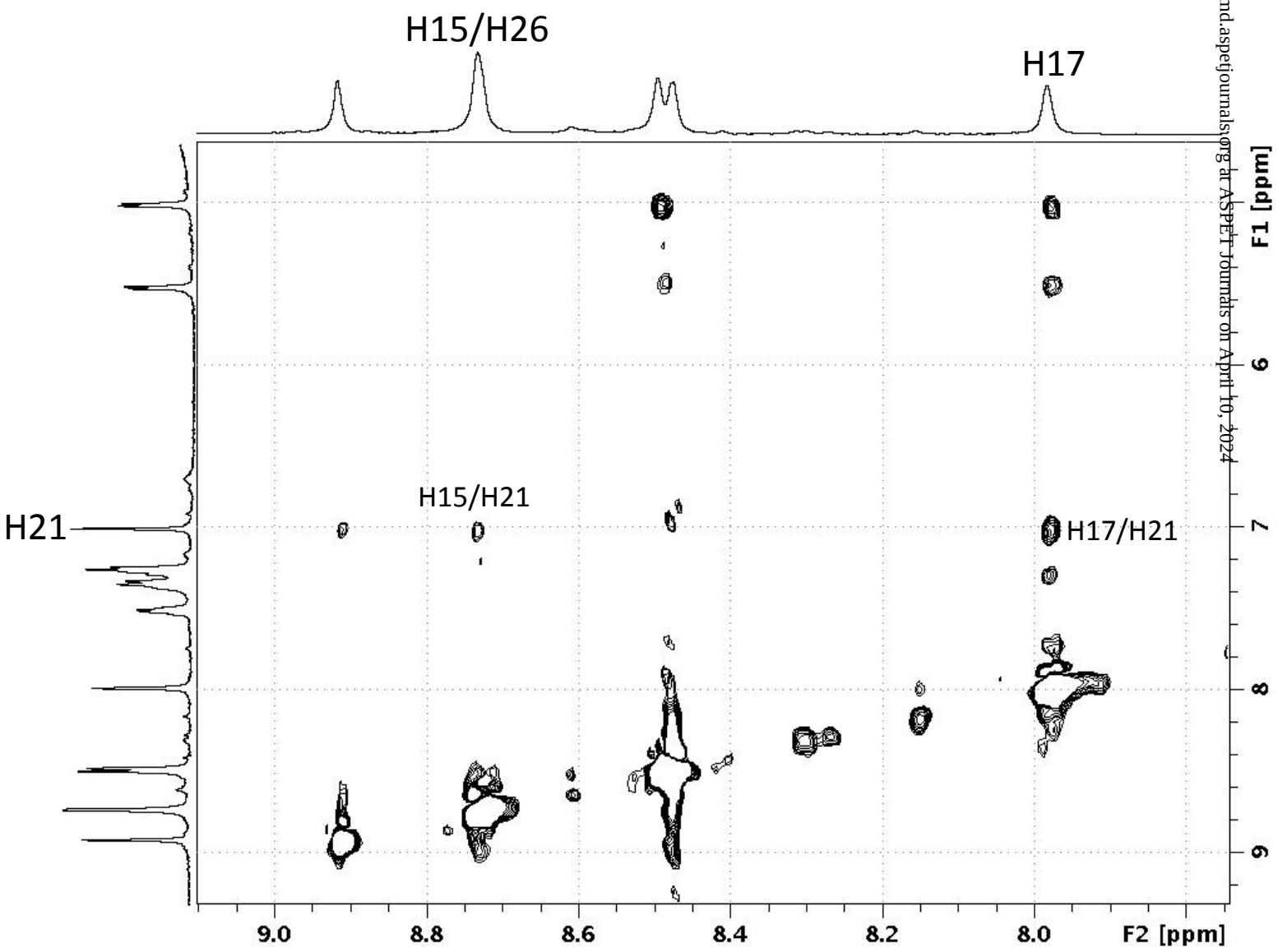

Figure 9

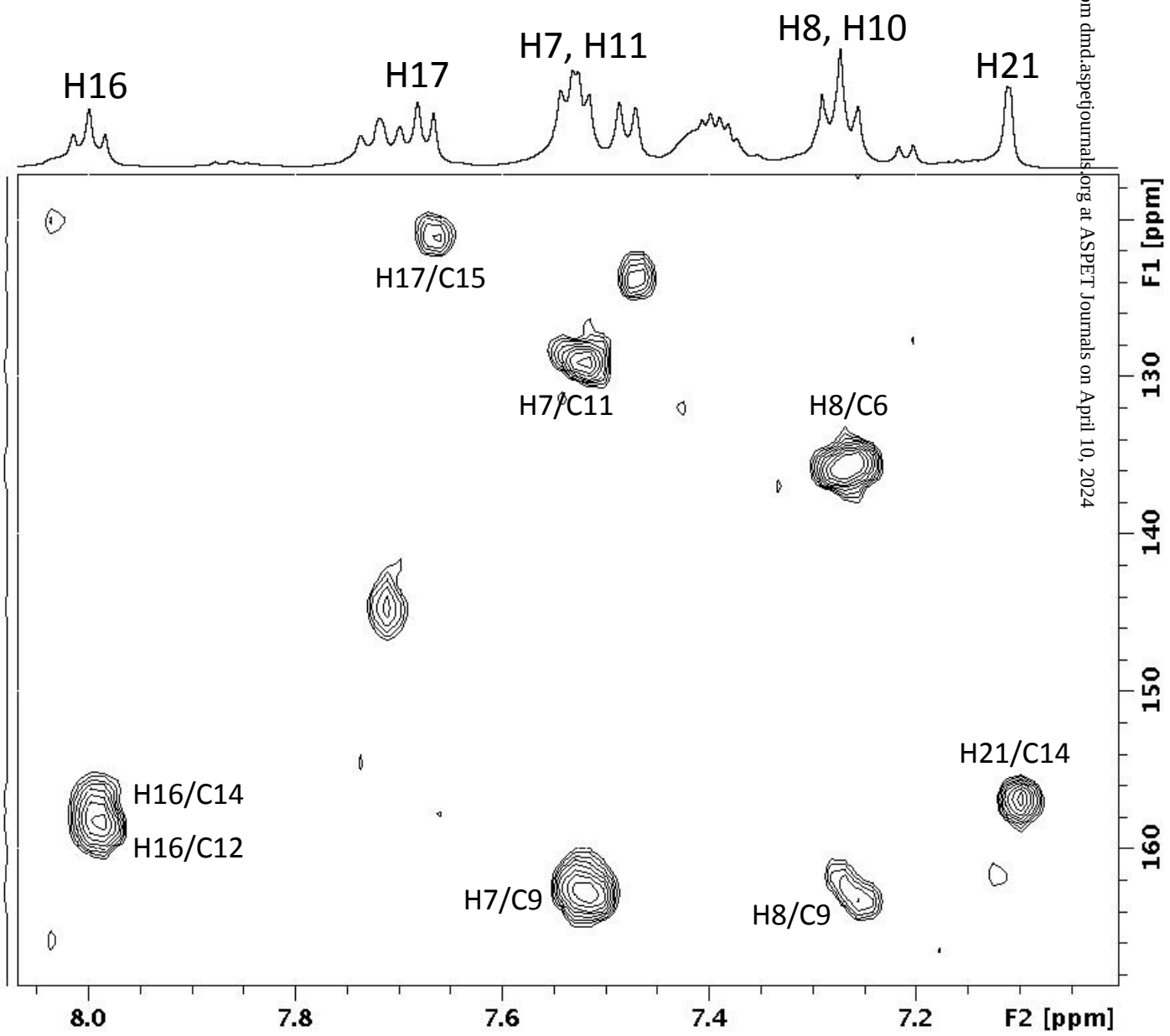

Figure 10

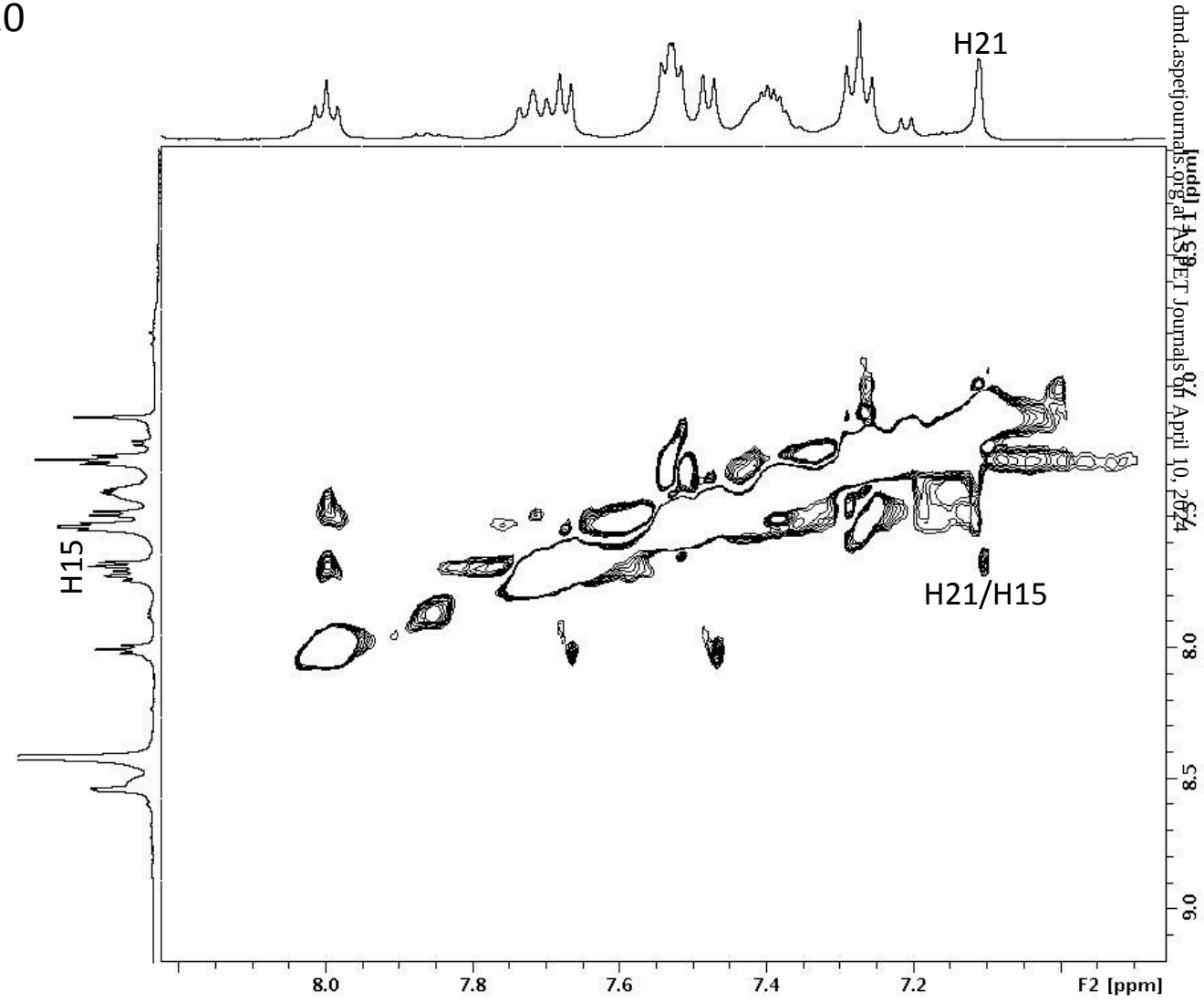

Figure 11